Celest Mech Dyn Astr (2009) 105:179–195
DOI 10.1007/s10569-009-9200-y

ORIGINAL ARTICLE

Non-Keplerian orbits for electric sails

Giovanni Mengali · Alessandro A. Quarta

Received: 15 September 2008 / Revised: 9 December 2008 / Accepted: 20 February 2009 /
Published online: 24 March 2009

Abstract An electric sail is capable of guaranteeing the fulfilment of a class of trajectories that would be otherwise unfeasible through conventional propulsion systems. In particular, the aim of this paper is to analyze the electric sail capabilities of generating a class of displaced non-Keplerian orbits, useful for the observation of the Sun's polar regions. These orbits are characterized through their physical parameters (orbital period and solar distance) and the spacecraft propulsion capabilities. A comparison with a solar sail is made to highlight which of the two systems is more convenient for a given mission scenario. The optimal (minimum time) transfer trajectories towards the displaced orbits are found with an indirect approach.

Keywords Electric sail · Displaced non-Keplerian orbit · Trajectory optimization · Solar sail

1 Introduction

An electric sail is an innovative propulsion concept that, similar to a more conventional solar sail, allows a spacecraft to deliver a payload to some high-energy orbit (McInnes 1999) without the need for reaction mass (Janhunen and Sandroos 2007). The spacecraft is spun around the symmetry axis (Mengali et al. 2008b) and the rotational motion is used to deploy approximately one hundred long conducting tethers (Fig. 1) held at a high positive potential through an electron gun, whose electron beam is shot roughly along the spin axis. The electric field generated by the tethers shields the spacecraft from the solar wind ions that, impacting on it, generate a continuous thrust that decays as $(1/r)^{7/6}$, where r is the Sun-sailcraft distance. To control the spacecraft thrust angle (defined as the angle between the thrust direction and the Sun-spacecraft line), the sail-plane attitude may be varied with the aid of potentiometers

G. Mengali (✉) · A. A. Quarta
Dipartimento di Ingegneria Aerospaziale, University of Pisa, Via G. Caruso 8, 56122 Pisa, Italy
e-mail: g.mengali@ing.unipi.it

A. A. Quarta
e-mail: a.quarta@ing.unipi.it

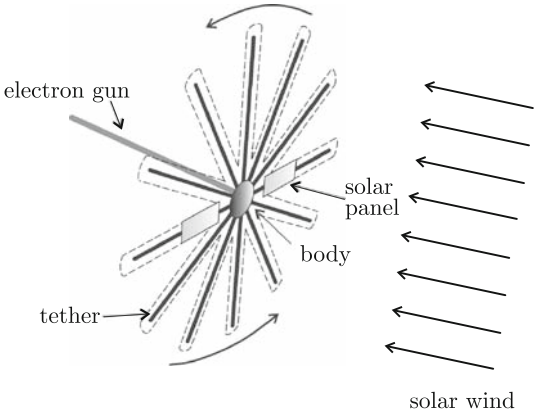

Fig. 1 Electric sail schematic view

placed between the spacecraft and each tether. For an in depth analysis of the electric sail performance, the reader is referred to Mengali et al. (2008b).

The theoretical availability of a propelling thrust for an unlimited time makes accessible a class of orbits (Mengali et al. 2008a; Racca 2004; Mengali and Quarta 2007) that would be otherwise very difficult or even infeasible through conventional propulsion systems (i.e., chemical or electrical). An important application is constituted by missions whose aim is to observe the Sun's polar regions, such as the Ulysses solar polar mission (Wenzel et al. 1992). These mission typologies, when achieved with chemical propulsion, require the use of highly elliptic trajectories of considerable inclination, whose fulfilment is typically obtained with the aid of complex multiple flyby maneuvers. An alternative consists of inserting a spacecraft in a nearly circular, non-Keplerian orbit (NKO), whose plane does not pass through the Sun's center of mass. Such a displaced NKO can be maintained by suitably orienting the thrust direction in such a way to balance the centrifugal and gravitational components of spacecraft acceleration. This class of orbits was studied by McInnes and Simmons (1992), Hughes and McInnes (2002), and McInnes (1997) as a possible application for solar sails but, currently no study involving the implementation of displaced orbits through electric sail is available.

The aim of this paper is to systematically analyze the potential of an electric sail to enable a class of NKO aimed at the observation of Sun's polar regions. In particular, the main NKO characteristics (in terms of orbital period and space direction) are related to the propulsion system capabilities (in terms of both acceleration and maximum thrust angle). Besides the study of optimal transfer trajectories towards the NKO, a performance comparison with an ideal solar sail is discussed.

2 Mathematical model

The equations of motion for an electric sailcraft in a heliocentric inertial frame $\mathcal{T}_\odot(x, y, z)$, with unit vectors $\hat{\boldsymbol{i}}$, $\hat{\boldsymbol{j}}$, $\hat{\boldsymbol{k}}$, are:

$$\dot{\boldsymbol{r}} = \boldsymbol{v} \tag{1}$$

$$\dot{\boldsymbol{v}} = -\frac{\mu_\odot}{r^3}\,\boldsymbol{r} + a_\oplus \left(\frac{r_\oplus}{r}\right)^\eta \hat{\boldsymbol{a}} \tag{2}$$

where $\boldsymbol{r}$, and $\boldsymbol{v}$ are the spacecraft position and velocity relative to $\mathcal{T}_\odot$ (with $r \triangleq \|\boldsymbol{r}\|$), $\mu_\odot = 132712439935.5\text{km}^3/\text{s}^2$ is the Sun's gravitational parameter, $\eta \triangleq 7/6$ (Janhunen and

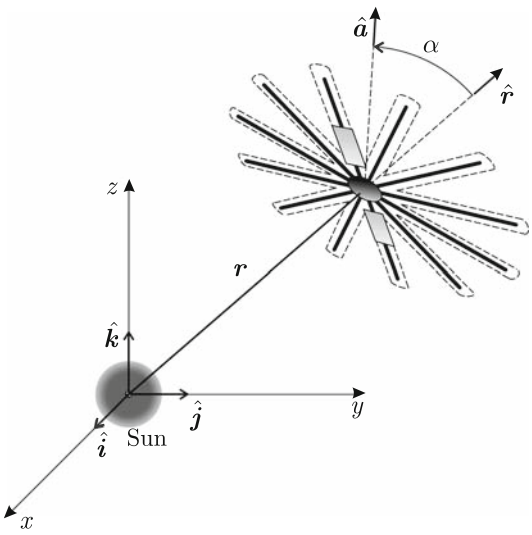

Fig. 2 Reference frame and cone angle

Sandroos 2007), $a_\oplus$ is the maximum sailcraft propulsive acceleration at $r = r_\oplus \triangleq 1$ AU and $\hat{\boldsymbol{a}}$ is the thrust unit vector. In analogy with the solar sail literature, $a_\oplus$ is called the electric sail characteristic acceleration.

Although an accurate analysis of the electric sail subsystems is not yet available, preliminary studies suggest that the maximum propelling acceleration, achievable in a near future at $r_\oplus = 1$ AU, is on the order of 2 mm/s^2. A reasonable estimate of $a_\oplus$, compatible with the current technology, is about 0.3–0.5 mm/s^2 (Janhunen and Sandroos 2007). Unlike electric thrusters, the propelling acceleration cannot be freely oriented, but it is constrained to lie within a cone whose axis coincides with the direction of the spacecraft position vector $\hat{\boldsymbol{r}} \triangleq \boldsymbol{r}/r$. In other terms (Fig. 2) the thrust direction forms an angle $\alpha \in [0,\ \alpha_{\max}]$ with respect to the position vector, where $\alpha_{\max} < \pi/2$ is the half-opening angle of the thruster operating cone (for an ideal solar sail, instead, $\alpha_{\max} = \pi/2$). The cone angle is given by:

$$\cos\alpha \triangleq \hat{\boldsymbol{r}} \cdot \hat{\boldsymbol{a}} \tag{3}$$

Although the maximum value of α is not known with confidence, the authors conjecture that it lies between 20° and 35°, based on numerical simulations. The electric sail thrust level depends on the solar wind properties, which are variable and cannot be estimated with confidence. To a large extent, however, these fluctuations can be compensated for by the electric thrust control, that is, by adjusting the electron gun current and voltage. Therefore, for the sake of simplicity, the solar wind variations are not taken into account in the present analysis.

The electric sail capability of generating a propelling thrust without any propellant consumption is useful for planning complex and interesting trajectories. A class of these trajectories is especially advisable for the study of the Sun's polar regions. To this end, consider an electric sail moving on a circular orbit of radius R, whose orbital plane is parallel to the ecliptic plane (x, y) (Fig. 3). Let $\omega \triangleq \|\boldsymbol{\omega}\|$ be the electric sail constant angular velocity, $T = 2\pi/\omega$ the corresponding orbital period, and h the out-of-plane displacement. Angle $\gamma \triangleq \arctan(h/R)$ defines the sail orientation with respect to the ecliptic plane and, therefore, the spacecraft horizon (Brown 1992).

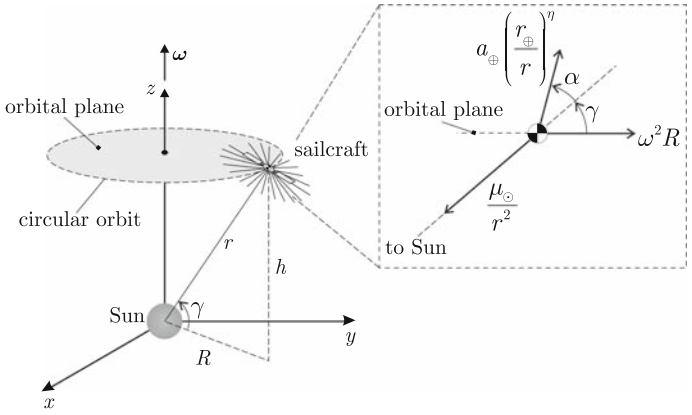

Fig. 3 Layout of displaced non-Keplerian orbit

Without loss of generality, in the following the spacecraft orbit will be assumed to belong to the half-space $z > 0$. Such a displaced orbit may be maintained by suitably orienting the propelling acceleration in such a way to balance the gravitational and the centrifugal acceleration (Fig. 3), viz.

$$a_\oplus \, (r_\oplus/r)^\eta \, \sin\alpha = \omega^2 \, R \, \sin\gamma \tag{4}$$

$$a_\oplus \, (r_\oplus/r)^\eta \, \cos\alpha + \omega^2 \, R \, \cos\gamma = \mu_\odot/r^2 \tag{5}$$

Let $\widetilde{\omega} \triangleq \sqrt{\mu_\odot/r^3}$ be the angular velocity of the Keplerian orbit of radius r. Assuming $\gamma \neq 0$, from Eqs. 4 to 5 the cone angle α and the characteristic acceleration $a_\oplus$ necessary to maintain a NKO are:

$$\tan\alpha = \frac{(\omega/\widetilde{\omega})^2 \, \tan\gamma}{1 + \tan^2\gamma \, - (\omega/\widetilde{\omega})^2} \tag{6}$$

$$\frac{a_\oplus}{\mu_\odot/r_\oplus^2} = \left(1 - \frac{(\omega/\widetilde{\omega})^2}{1+\tan^2\gamma}\right) \sqrt{1 + \frac{\tan^2\gamma}{\left[\left(1+\tan^2\gamma\right)/(\omega/\widetilde{\omega})^2 - 1\right]^2}} \left(\frac{r_\oplus}{r}\right)^{2-\eta} \tag{7}$$

where $\mu_\odot/r_\oplus^2 \cong 5.93\,\mathrm{mm/s^2}$ is the solar gravitational acceleration at 1 AU. In particular, Eq. 6 coincides with that found by McInnes and Simmons (1992) for solar sails.

Some remarks about the admissible combinations of γ and $(\widetilde{\omega}/\omega)$ are in order. Consider the family of orbits, referred to as Type II by McInnes (1999), characterized by a non-Keplerian orbital period equal to the Keplerian period (i.e., these orbits are synchronous with the Keplerian circular orbits having radius r). The mathematical condition for Type II orbits is, therefore, $\omega = \widetilde{\omega}$. Assuming an electric sail cone angle constraint $\alpha_{\max} = 35°$, from Fig. 4 (equivalently from Eq. 6), one concludes that a Type II orbit may be obtained only provided that the sail orientation angle γ is greater than 55°. Figure 5 shows the corresponding values of characteristic acceleration. A displaced NKO at Earth's distance needs a characteristic acceleration greater than $4.8\,\mathrm{mm/s^2}$.

The particular case $\gamma = 0$ deserves a separate discussion. First observe that the condition $\gamma = 0$ corresponds to orbits belonging to the ecliptic plane ($h = 0$). Equation (4) shows that $\gamma = 0$ implies $\alpha = 0$, while from Fig. 3 it is clear that $h = 0$ implies $r \equiv R$. Therefore, the equilibrium condition in Eq. 5 becomes

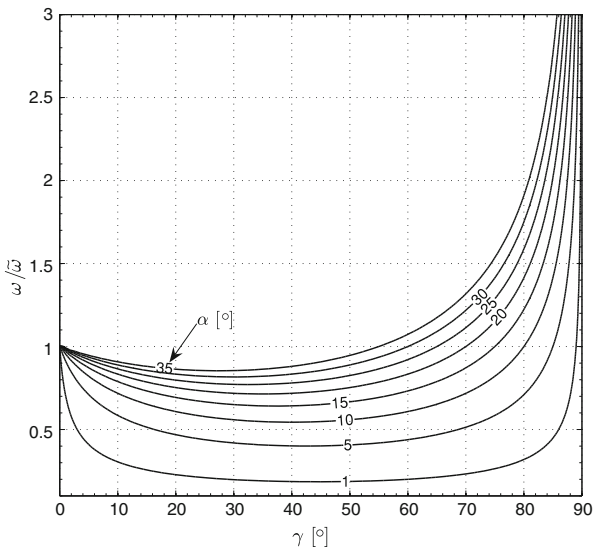

Fig. 4 Sailcraft cone angle α along the displaced orbit as a function of γ, and $(\omega/\widetilde{\omega})$, see Eq. 6

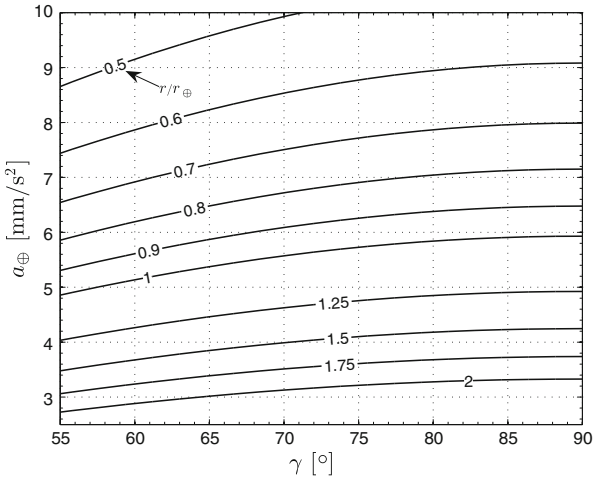

Fig. 5 Characteristic acceleration necessary to maintain a Type II NKO as a function of γ, and $r/r_\oplus$

$$\frac{a_\oplus}{\mu_\odot/r_\oplus^2} = \left[1 - \left(\frac{\omega}{\widetilde{\omega}}\right)^2\right] \left(\frac{r_\oplus}{r}\right)^{2-\eta} \tag{8}$$

For a given angular velocity ω (or orbital period $T = 2\pi/\omega$), Eq. 8 provides the relationship between the distance r and the corresponding characteristic acceleration $a_\oplus$ necessary to maintain an equatorial NKO. In particular, note that $\omega = \sqrt{\mu_\odot/r^3}$ implies $a_\oplus = 0$ because, in that case, one obtains a circular Keplerian orbit. Figure 6 shows that it is possible to generate an in-plane, artificial Earth-synchronous NKO, that is, an orbit having orbital period $T = 1$ year, even for $r < 1$ AU, provided that the characteristic acceleration is sufficiently high.

Another particular situation is obtained for $\gamma = \pi/2$, that is, when the electric sail is placed on the z-axis of the reference frame $\mathcal{T}_\odot(x, y, z)$. In this case the orbit degenerates

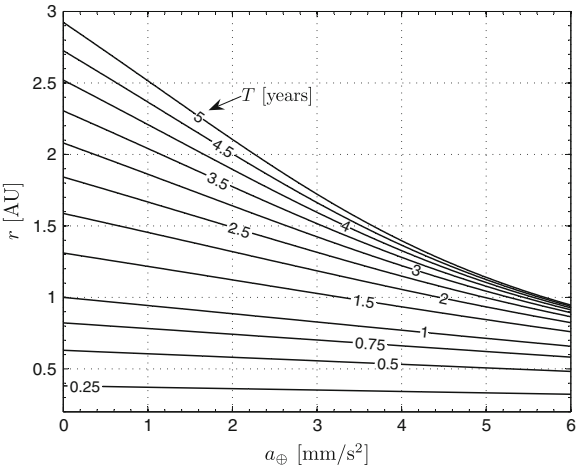

Fig. 6 NKO radius of ecliptic orbits ($\gamma = 0$) as a function of the sailcraft characteristic acceleration $a_\oplus$, and orbital period T

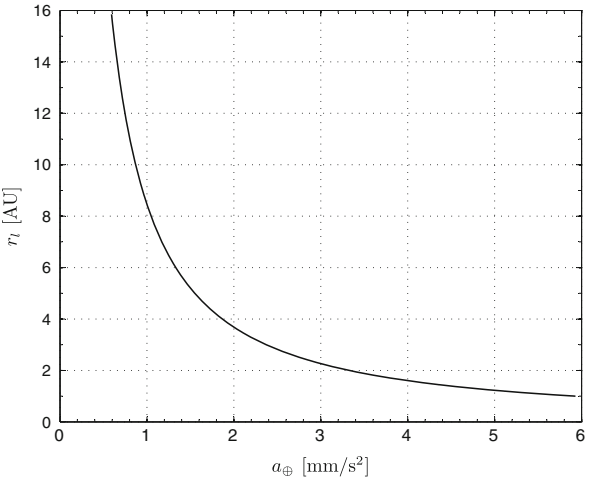

Fig. 7 Sailcraft performance ($a_\oplus$) for heliostationary orbit (radius r_l), see Eq. 9

in a point and the sail levitates over the Sun's pole at a distance r_l from the Sun's center of mass. This condition, although optimal for observing the solar polar region, can be satisfied for distances <1 AU only with very high performance electric sails. In fact, from the balance equation between the propelling acceleration $a_\oplus \, (r_\oplus / r_l)^\eta$ and the solar gravitational attraction $\mu_\odot / r_l^2$ (Eq. 8), the equilibrium distance r_l is found to be

$$r_l = r_\oplus \left(\frac{a_\oplus}{\mu_\odot / r_\oplus^2} \right)^{1/(\eta-2)} \tag{9}$$

Note that Eq. 9 can also be obtained from Eq. 7 in the limit as $\gamma \to \pi/2$. Assuming $a_\oplus \leq 1\,\mathrm{mm/s^2}$, Fig. 7 shows that the heliostationary condition may be obtained above 8.5 AU, a sizeable distance from the Sun. With the current technology, assuming $a_\oplus \leq 0.5\,\mathrm{mm/s^2}$, condition (9) implies a very large distance from the Sun, on the order of 20 AU, that is, approximately the same distance as Uranus' orbit radius.

Return now to Eqs. 6–7. These two equations allow one to obtain the thrust direction and estimate the sail performance (in terms of $a_\oplus$) as a function of the triplet (γ, r, ω). For a given

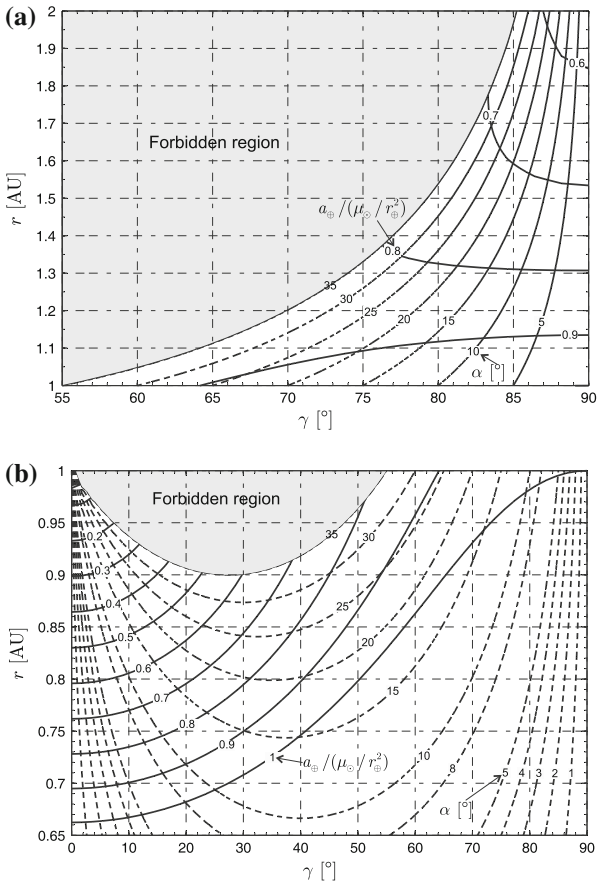

Fig. 8 Sailcraft performance for NKO with $T = 1$ year, and $\alpha_{\max} = 35°$ ($\mu_\oplus/r_\oplus^2 = 5.93\,\text{mm/s}^2$). **a** $r > 1$ AU. **b** $r < 1$ AU

value of orbital period or angular velocity of the NKO, the information contained in Eqs. 6–7 may be consolidated and collected in graphical form. For example, assuming $\alpha_{\max} = 35°$, and $T = 1$ year (that is, $\omega = 2\,\pi$ rad/year) the result is shown in Fig. 8. For the sake of clarity, the information concerning inner (Fig. 8a) and outer (Fig. 8b) orbits have been separated.

Figure 8b shows that an Earth-synchronous NKO with a sufficient view angle (on the order of $\gamma = 65°$) and having a solar distance of 0.9 AU, requires a very high characteristic acceleration, that is $a_\oplus \cong 6\,\text{mm/s}^2$. Using an electric sail of medium–high performance, with $a_\oplus \in [1,\ 2]\,\text{mm/s}^2$, it is possible to generate a displaced NKO with a rather small view angle ($\gamma < 12°$) at a solar distance close to 1 AU.

3 Optimal orbit transfer

Having analyzed different NKO as a function of both sail characteristics (in terms of $a_\oplus$, and $\alpha_{\max}$) and orbit type (r, T, and γ), we are now in a position to discuss the problem of transfer trajectory. In particular, the transfer problem is addressed in an optimal framework, that is, by minimizing the flight time necessary to transfer the spacecraft from a given parking orbit to the desired final NKO. To simplify our discussion, an initial circular parking orbit

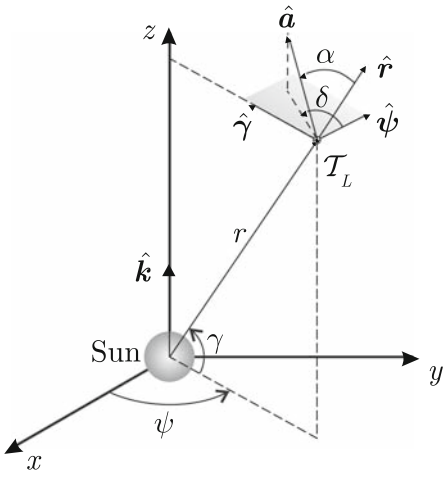

Fig. 9 Heliocentric spherical coordinate system

is considered. The orbit has radius $r_\oplus$, and is assumed to belong to the ecliptic plane. This situation is representative of a sailcraft deployment on a parabolic Earth escape trajectory, that is, with zero hyperbolic excess energy.

Due to the problem symmetry, the equations of motions (1)–(2) can be suitably expressed through a spherical coordinate system $\mathcal{T}_\odot(r, \psi, \gamma)$, where ψ is the ecliptic longitude, measured anticlockwise from x axis.

With reference to Fig. 9 and with the aid of Wie (2007), the following equations of motion are obtained:

$$\dot{r} = v_r \tag{10}$$

$$\dot{\psi} = \frac{v_\psi}{r\,\cos\gamma} \tag{11}$$

$$\dot{\gamma} = \frac{v_\gamma}{r} \tag{12}$$

$$\dot{v}_r = \frac{v_\psi^2 + v_\gamma^2}{r} - \frac{\mu_\odot}{r^2} + \tau\, a_r \tag{13}$$

$$\dot{v}_\psi = \frac{v_\psi\, v_\gamma\, \tan\gamma - v_r\, v_\psi}{r} + \tau\, a_\psi \tag{14}$$

$$\dot{v}_\gamma = -\frac{v_\psi^2\, \tan\gamma + v_r\, v_\gamma}{r} + \tau\, a_\gamma \tag{15}$$

In Eqs. 13–15, $\tau = (0, 1)$ is the thruster switching function, which allows one to model the presence of coasting arcs in the spacecraft trajectory. To define the sail acceleration orientation, it is convenient to introduce a local orbital frame $\mathcal{T}_L\,(x_L, y_L, z_L)$, with unit vectors defined as (Fig. 9)

$$\hat{\boldsymbol{i}}_L = \hat{\boldsymbol{r}}, \quad \hat{\boldsymbol{j}}_L = \hat{\boldsymbol{k}} \times \hat{\boldsymbol{r}}, \quad \hat{\boldsymbol{k}}_L = \hat{\boldsymbol{i}}_L \times \hat{\boldsymbol{j}}_L \tag{16}$$

The projection of $\hat{\boldsymbol{a}}$ in the plane (y_L, z_L) defines the sail clock angle $\delta \in [0,\ 2\,\pi]$, measured anticlockwise from the y_L axis. The components of the thrust acceleration with respect to $\mathcal{T}_L$ are given by

$$[\boldsymbol{a}]_{\mathcal{T}_L} = \begin{bmatrix} a_r \\ a_\psi \\ a_\gamma \end{bmatrix} \triangleq a_\oplus \left(\frac{r_\oplus}{r}\right)^\eta \begin{bmatrix} \cos\alpha \\ \sin\alpha\ \cos\delta \\ \sin\alpha\ \sin\delta \end{bmatrix} \tag{17}$$

The minimum transfer time $\Delta t = t_f - t_0 \equiv t_f$ is calculated using an indirect technique, by maximizing the scalar functional J defined as

$$J \triangleq -t_f \tag{18}$$

Recalling the equations of motion (10)–(15), the Hamiltonian H is given by:

$$\begin{aligned} H \triangleq & \lambda_r\, v_r + \lambda_\psi \frac{v_\psi}{r\,\cos\gamma} + \lambda_\gamma \frac{v_\gamma}{r} + \lambda_{v_r}\left(\frac{v_\psi^2 + v_\gamma^2}{r} - \frac{\mu_\odot}{r^2}\right) \\ & + \lambda_{v_\psi} \frac{v_\psi\, v_\gamma\, \tan\gamma - v_r\, v_\psi}{r} - \lambda_{v_\gamma} \frac{v_\psi^2\, \tan\gamma + v_r\, v_\gamma}{r} + H' \end{aligned} \tag{19}$$

where $\lambda_r, \lambda_\psi, \lambda_\gamma, \lambda_{v_r}, \lambda_{v_\psi}$, and λ_{v_γ} are the adjoint variables and H' coincides with that portion of the Hamiltonian H that explicitly depends on the control vector $\boldsymbol{u} \triangleq [\tau,\ \alpha,\ \delta]^{\mathrm{T}}$, that is

$$H' \triangleq a_\oplus\, \tau \left[\lambda_{v_r}\, \cos\alpha + \lambda_{v_\psi}\, \sin\alpha\, \cos\delta + \lambda_{v_\gamma}\, \sin\alpha\, \sin\delta\right] \left(\frac{r_\oplus}{r}\right)^\eta \tag{20}$$

The time derivative of j-th adjoint variable is obtained from the Euler–Lagrange equations:

$$\dot{\lambda}_j = -\frac{\partial H}{\partial j} \quad \text{with} \quad j \triangleq (r,\ \psi,\ \gamma,\ v_r,\ v_\psi,\ v_\gamma) \tag{21}$$

Evaluating Eq. 21 using Eqs. 19 and 20 yields:

$$\dot{\lambda}_r = \frac{H - H' - \lambda_r\, v_r - \lambda_{v_r}\, \mu_\odot / r^2}{r} + \frac{\eta\, H'}{r} \tag{22}$$

$$\dot{\lambda}_\psi = 0 \tag{23}$$

$$\dot{\lambda}_\gamma = \frac{v_\psi \left(\lambda_{v_\gamma}\, v_\psi - \lambda_{v_\psi}\, v_\gamma - \lambda_\psi\, \sin\gamma\right)}{r\, \cos^2\gamma} \tag{24}$$

$$\dot{\lambda}_{v_r} = -\lambda_r + \frac{\lambda_{v_\psi}\, v_\psi + \lambda_{v_\gamma}\, v_\gamma}{r} \tag{25}$$

$$\dot{\lambda}_{v_\psi} = \frac{2\left(\lambda_{v_\gamma}\, v_\psi\, \tan\gamma - \lambda_{v_r}\, v_\psi\right) - \lambda_{v_\psi}\left(v_\gamma\, \tan\gamma - v_r\right)}{r} - \frac{\lambda_\psi}{r\, \cos\gamma} \tag{26}$$

$$\dot{\lambda}_{v_\gamma} = -\frac{\lambda_\gamma + 2\,\lambda_{v_r}\, v_\gamma + \lambda_{v_\psi}\, v_\psi\, \tan\gamma - \lambda_{v_\gamma}\, v_r}{r} \tag{27}$$

From the Pontryagin's maximum principle, the optimal control law $\boldsymbol{u}(t)$, to be selected in the domain of feasible controls $\mathcal{U}$, is such that, at any time, the function H' is an absolute maximum:

$$\boldsymbol{u} = \max_{\boldsymbol{u} \in \mathcal{U}} H' \tag{28}$$

Invoking the necessary conditions $\partial H'/\partial\alpha = 0$, and $\partial H'/\partial\delta = 0$, the following relationships for the thrust angles are obtained:

$$\alpha = \begin{cases} \alpha^\star & \text{if} \quad \alpha^\star \le \alpha_{\max} \\ \alpha_{\max} & \text{if} \quad \alpha^\star > \alpha_{\max} \end{cases} \quad \text{with} \quad \cos\alpha^\star \triangleq \frac{\lambda_{v_r}}{\sqrt{\lambda_{v_r}^2 + \lambda_{v_\psi}^2 + \lambda_{v_\gamma}^2}} \tag{29}$$

$$\cos\delta = \frac{\lambda_{v_\psi}}{\sqrt{\lambda_{v_\psi}^2 + \lambda_{v_\gamma}^2}}, \quad \sin\delta = \frac{\lambda_{v_\gamma}}{\sqrt{\lambda_{v_\psi}^2 + \lambda_{v_\gamma}^2}} \tag{30}$$

Note that the optimal control law (29) and (30) is the three-dimensional extension of the analogous (bi-dimensional) result discussed by Mengali et al. (2008b). The optimal control law for the switching function is found observing that H' depends linearly on τ. As a result, a bang-bang control is optimal (Stengel 1986):

$$\tau = \frac{1 + \text{sign}\,(s_w)}{2} \quad \text{with} \quad s_w \triangleq \lambda_{v_r}\cos\alpha + \sin\alpha\sqrt{\lambda_{v_\psi}^2 + \lambda_{v_\gamma}^2} \tag{31}$$

where sign $(\cdot)$ is the signum function and α is given by Eq. 29.

The boundary-value problem associated to the variational problem is constituted by the equations of motion (10)–(15) and by the Euler–Lagrange equations 22–27. The corresponding 12 boundary conditions are connected to the desired spacecraft position and velocity at both the initial ($t_0 = 0$) and final (t_f) time.

Let r_f, γ_f, and ω be the given characteristic parameters of the final displaced NKO. Recalling that the initial parking orbit is circular with radius $r_\oplus = 1$ AU, one has:

$$t = t_0 \quad : \quad r = r_\oplus, \quad \psi \equiv \gamma \equiv v_r \equiv v_\gamma = 0, \quad v_\psi = \sqrt{\mu_\odot / r_\oplus} \tag{32}$$

$$t = t_f \quad : \quad r = r_f, \quad v_r \equiv v_\gamma \equiv \lambda_\psi = 0, \quad \gamma = \gamma_f, \quad v_\psi = \omega r_f \cos\gamma_f \tag{33}$$

In Eq. 32, the condition $\psi(t_0) = 0$ is enforced in view of the problem symmetry and all $\lambda_j(t_0)$ are free, while the condition $\lambda_\psi(t_f) = 0$ in (33) is due to the fact that the angular position ψ on the displaced NKO is an output of the optimization process. Also note, from Eq. 23, that the adjoint variable λ_ψ is constant along the optimal trajectory and, therefore, $\lambda_\psi = 0$ during the whole transfer. The transversality condition $H(t_f) = 1$, necessary to determine the optimal value of t_f, completes the differential problem (Bryson and Ho 1975).

The optimal control law, given by Eqs. 29–30, has been used to calculate the minimum time transfer trajectories towards a displaced NKO of given characteristics in terms of r_f, γ_f, and T. Assuming an Earth-synchronous orbit ($T = 1$ year), and a solar distance $r_f = 0.9$ AU, the minimum transfer times t_f have been calculated as a function of the view angle in the range $\gamma_f \in [1°,\ 28°]$. In all of the simulations, the differential equations have been integrated in double precision using a variable order Adams–Bashforth–Moulton solver (i.e., Matlab's ODE113) with absolute and relative errors of 10^{-12}. The simulation results of the optimal transfers have been summarized in Fig. 10. The choice about the value of γ_f is essentially related to the value of characteristic acceleration required to maintain the given displaced orbit. In fact, Figs. 8b and 10c show that $\gamma_f > 28°$ corresponds to an extremely high value of characteristic acceleration, that is, $a_\oplus > 3.5\,\text{mm/s}^2$ (see also Eq. 7).

For example, assuming $\gamma_f = 25°$, $T = 1$ year, and $r_f = 0.9$ AU (which corresponds to a displaced orbit with a height $h = r_f \sin\gamma_f \cong 0.38$ AU with respect to the ecliptic plane), the optimal transfer time is $t_f \cong 201$ days and the required characteristic acceleration is $a_\oplus \cong 3.16\,\text{mm/s}^2$. The time history for the control angles $\alpha = \alpha(t)$ and $\delta = \delta(t)$ is illustrated in Fig. 11. The presence of a coasting phase of about 50 days, starting 40 days after the departure, is due to the constraint on the maximum value of the cone angle. This coasting phase is also visible in Fig. 12, which shows the sailcraft transfer trajectory.

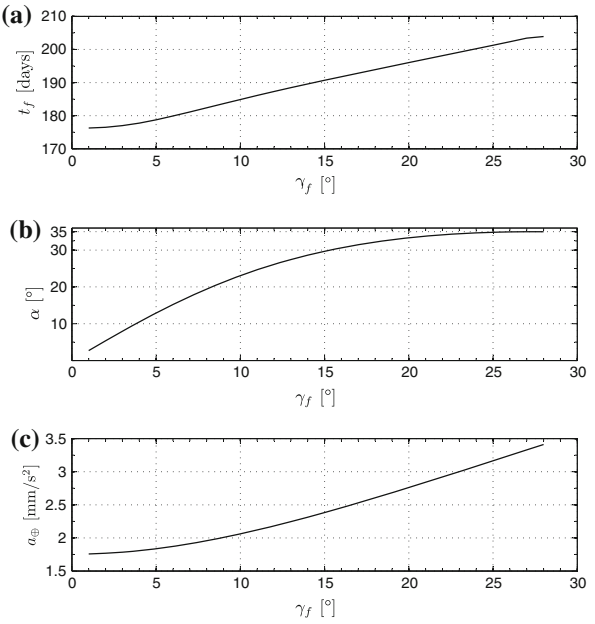

Fig. 10 Minimum time NKO transfer as a function of γ_f ($T = 1$ year and $r_f = 0.9$ AU). **a** Flight time. **b** Sail cone angle, see Eq. 6. **c** Characteristic acceleration, see Eq. 7

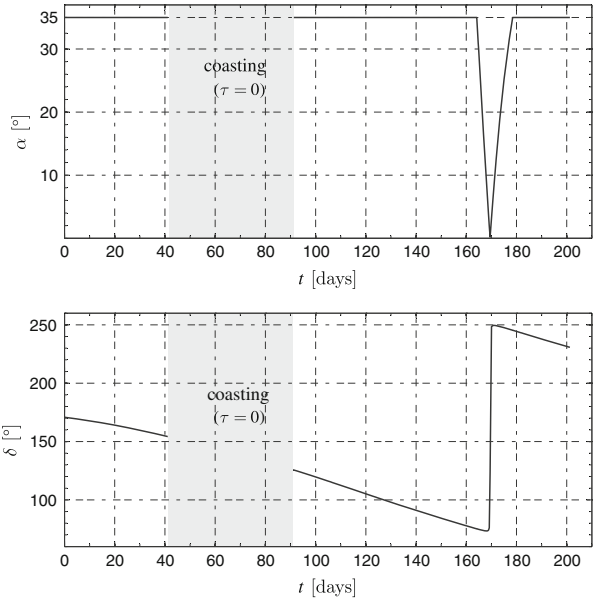

Fig. 11 Time histories of control angles α and δ for a minimum time transfer trajectory ($\gamma_f = 25°$, $T = 1$ year, and $r_f = 0.9$ AU)

4 Numerical response to perturbations

For the sake of completeness, and in analogy with solar sail literature, it is interesting to introduce the problem of displaced orbit sensitivity to perturbations. In fact, the previous analysis does not take into account any disturbance and is based on the exact fulfilment of the equilibrium relationships given by Eqs. 6–7. Unlike the stability study proposed in

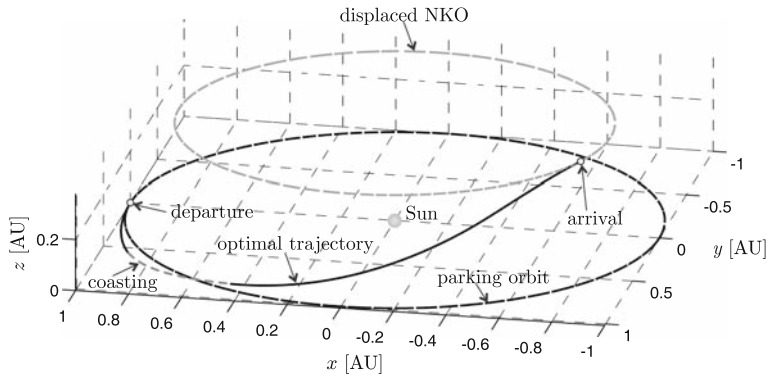

Fig. 12 Sailcraft optimal trajectory ($\gamma_f = 25°$, $T = 1$ year, and $r_f = 0.9$ AU). The whole trajectory takes place in the half-space $z > 0$

McInnes (1998), where the equations of motion are linearized with respect to the nominal orbit, here the behavior of NKO with respect to perturbations is tackled by simulation, using the full nonlinear equations of motion. The aim is to investigate the capability for a spacecraft of maintaining a displaced orbit within acceptable tolerances during the whole operational life.

Although the following analysis is confined to study the effect of a position error alone on the motion characteristics, it may be easily extended to the other parameters of concern with minor adjustments. The approach consists in slightly modifying the nominal equilibrium distance r_{nom} (which, by definition, satisfies Eqs. 6–7), replacing it with a perturbing value in the form $r(t_0) = r_{\text{nom}} \times 1.001$. The nonlinear differential equations of motion are then propagated for a given time interval (in our simulations $t_f = 3$ years) and the spacecraft position at the end of simulation is calculated.

A viable trajectory is associated to the fulfilment of the condition $r(t_f)/r(t_0) < 1.01$, or when the difference between final and initial distance does not exceed 1/100 of the initial nominal value. The results of this analysis are summarized in Fig. 13 (which is in accordance with Fig. 8b). Note that the nominal trajectory shown in the previous example ($\gamma_f = 25°$, $T = 1$ year, and $r_f = 0.9$ AU) is in the region in which $r(t_f)/r(t_0) > 1.01$. This result is confirmed by the simulations shown in Fig. 14. Such a displaced orbit would require the employment of an active control system. This study, however, is beyond the scope of this paper and is left to future research.

5 Electric sail versus solar sail

Similar to electric sails, solar sails are capable of generating propelling thrust by suitably converting the energy coming from the Sun without the need of any propellant. A solar sail is a large, lightweight and reflective surface, essentially a large space mirror (McInnes and Brown 1990), which is able to propel a spacecraft through the momentum transfer from photons that, emitted by the Sun, strike the sail. A solar sail may display a rather complex and, in general, not plane shape (Kirpichnikov et al. 2004; Mengali and Quarta 2005a,b, 2006). Under the simplified assumption that the sail surface is plain, it may be shown (McInnes 1999; Wright 1992) that the propelling thrust varies as the inverse square distance from the

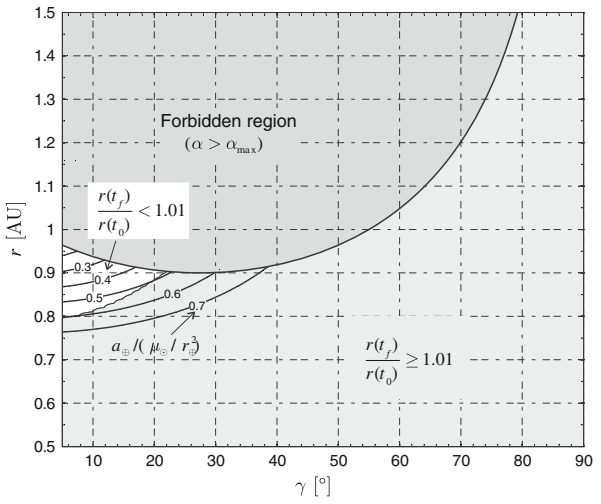

Fig. 13 Numerical analysis to position perturbations of electric sail displaced orbits with period $T = 1$ year($t_0 = 0, t_f = 3$ years)

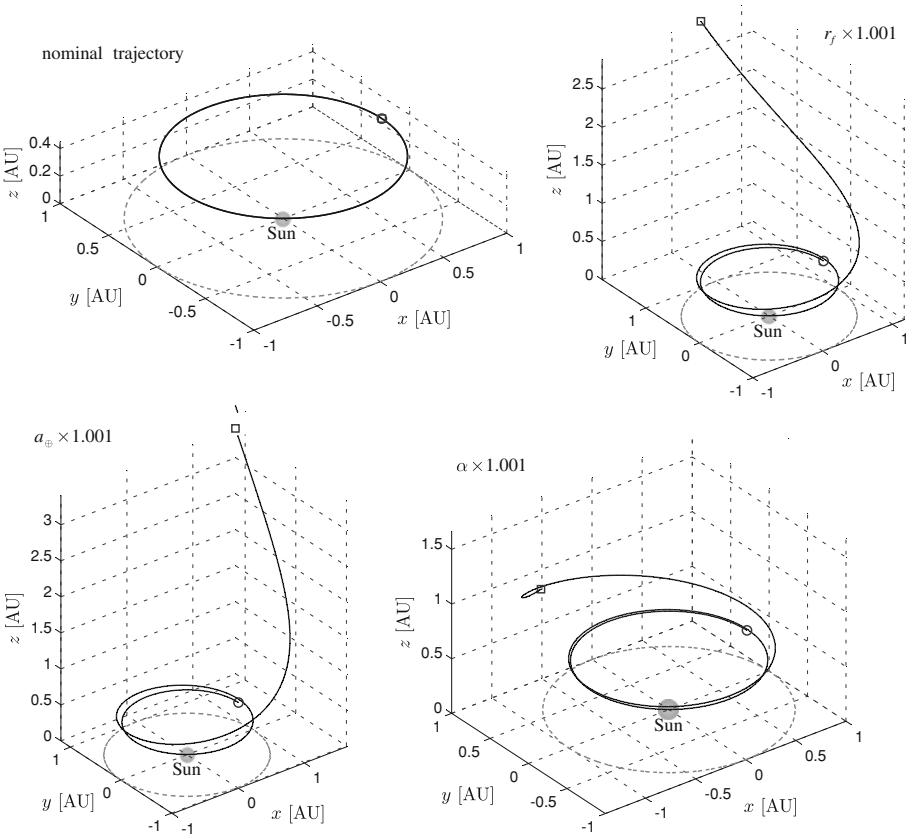

Fig. 14 Comparison of nominal and perturbed displaced orbits for a time span of 3 years(o $\equiv t_0 = 0$, $\square \equiv t_f = 3$ years). The nominal orbital parameters are $\gamma_f = 25°$, $T = 1$ year, and $r_f = 0.9$ AU

Sun and its value is a function of the cone angle α, that is, the angle between the Sun-sailcraft direction $\hat{\boldsymbol{r}}$ and the normal to the sail plane $\hat{\boldsymbol{n}}$ in the direction of thrust.

Unlike electric sails, the maximum value of the cone angle is not constrained by instability reasons, but from the fact that the thrust is always directed away from the Sun. As a result, $\alpha_{\max} = 90°$. The solar sail performance is characterized by the value of the characteristic acceleration $a_\oplus$, defined as the maximum developable acceleration at $r = r_\oplus \triangleq 1$ AU, and $\alpha = 0$.

Assuming a perfectly reflecting sail film, it may be shown (Wright 1992; Mengali et al. 2007) that the propelling acceleration is given by:

$$\boldsymbol{a}_{\mathrm{SS}} = a_\oplus \left(\frac{r_\oplus}{r}\right)^2 \cos^2\alpha\, \hat{\boldsymbol{n}} \tag{34}$$

In particular, note that the net thrust vanishes when $\alpha = \alpha_{\max} \triangleq 90°$, because in that case the sail plane is parallel to the incident rays. Decomposing the dimensionless acceleration $\boldsymbol{a}_{\mathrm{SS}}/a_\oplus$ along the radial and transversal directions, the results can be collected in graphical form. This is done in Fig. 15, in which the electric sail and solar sail performance are compared under the assumption of same solar distance $r = r_\oplus$. From Eq. 34, the differential equation of motion for a solar sail is given by (Kim and Hall 2005; Koblik et al. 2003; Van Der Ha and Modi 1979):

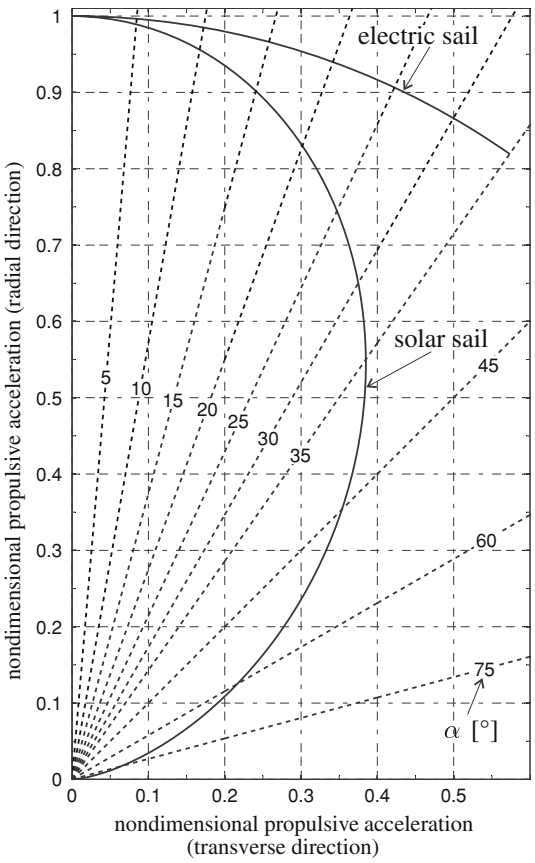

Fig. 15 Solar sail versus electric sail performance in terms of dimensionless propulsive acceleration components $\boldsymbol{a}/a_\oplus$ when $r = r_\oplus$

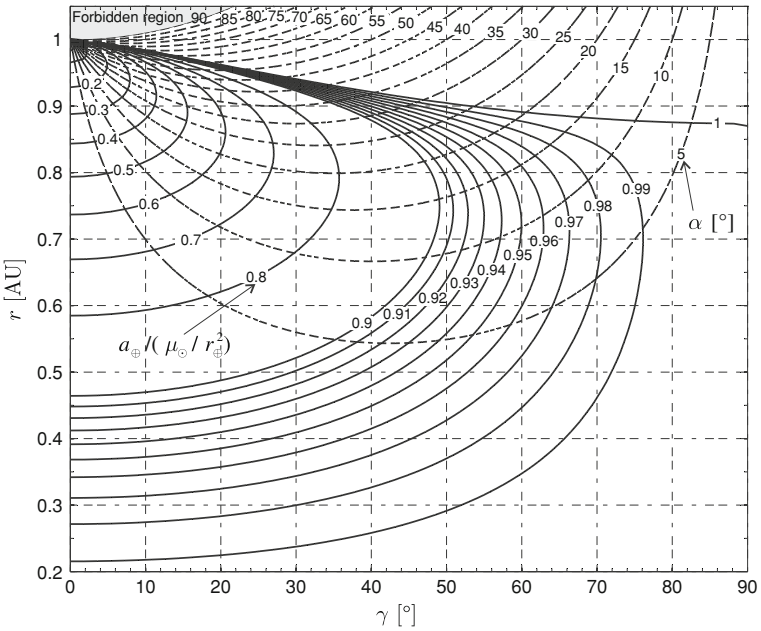

Fig. 16 Solar sail performance in terms of dimensionless propulsive acceleration components $\boldsymbol{a}_{SS}/a_\oplus$ when $r = r_\oplus$

$$\ddot{\boldsymbol{r}} = -\frac{\mu_\odot}{r^3}\,\boldsymbol{r} + a_\oplus \left(\frac{r_\oplus}{r}\right)^2 \cos^2\alpha\,\hat{\boldsymbol{n}} \tag{35}$$

Using the same technique used for electric sails, it is possible to obtain the relationships, for both the cone angle and the characteristic acceleration, necessary to maintain a displaced NKO of given characteristics (Baoyin and Mcinnes 2006). It may be shown (McInnes and Simmons 1992), that α satisfies a relationship identical to Eq. 6, while as long as $a_\oplus$ is concerned, the result is:

$$\frac{a_\oplus}{\mu_\odot/r_\oplus^2} = \frac{\left\{\tan^2\gamma + \left[1-(\omega/\widetilde{\omega})^2\right]^2\right\}^{3/2}}{\left[\tan^2\gamma + 1 - (\omega/\widetilde{\omega})^2\right]^2}\sqrt{1+\tan^2\gamma} \tag{36}$$

Note that the required characteristic acceleration of a solar sail NKO is a function of two parameters only, γ and $\omega/\widetilde{\omega}$, and, in particular, unlike electric sails, does not depend on r. The reason for this difference is that the solar sail propelling acceleration varies with the distance in the same way as the solar gravitational attraction.

For a given value of the NKO period, Eqs. 6 and 36 can be collected in a single graph. The results obtained for an Earth-synchronous orbit ($T = 1$ year) are shown in Fig. 16.

Unlike electric sails (Fig. 8), as long as $a_\oplus/(\mu_\odot/r_\oplus^2) < 1$, the solar sail NKO are characterized by $r < 1$ AU. Nevertheless, thanks to the inverse quadratic relationship between thrust and distance, solar sails are capable of maintaining NKO using characteristic accelerations smaller than those corresponding to electric sails when small values of γ and r are sought. On the other hand, for distances close to $r_\oplus$ and wide view angles an electric sail is superior because the required characteristic acceleration is smaller.

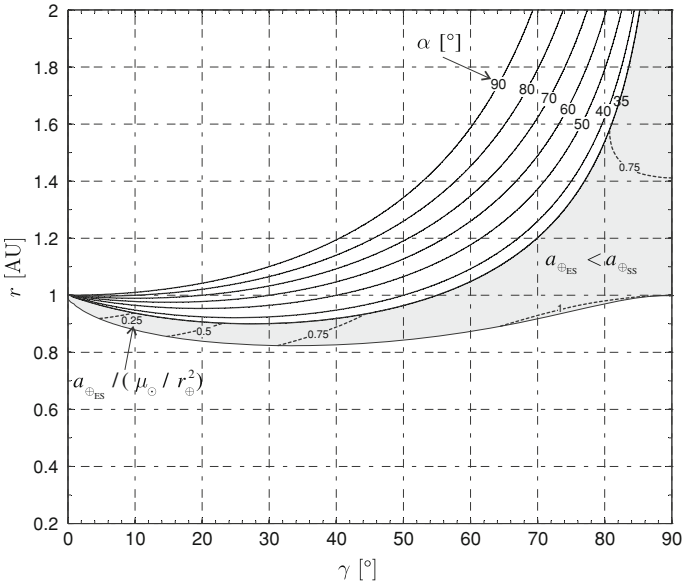

Fig. 17 Solar sail versus electric sail performance for displaced NKO orbit with $T = 1$ year. The region where the electric sail's characteristic acceleration is less than that of the solar sail is highlighted in gray

Assuming $T = 1$ year, Eqs. 7 and 36 allow one to locate the space regions, in the plane (r, γ), in which the electric sail performance is superior to a solar sail in the sense that $a_{\oplus ES} < a_{\oplus SS}$. This situation is summarized in Fig. 17. For example, an Earth-synchronous displaced NKO with radius $r = 0.9$ AU and view angle $\gamma = 50°$ requires a solar sail characteristic acceleration $a_{\oplus SS}/(\mu_\odot/r_\oplus^2) \cong 0.993$ and a cone angle $\alpha \cong 27.2°$, while, for an electric sail, $a_{\oplus ES}/(\mu_\odot/r_\oplus^2) \cong 0.857$ (which is 14% less than that of the solar sail).

6 Conclusions

Electric sails may be used effectively to generate families of displaced non-Keplerian orbits. These orbits are maintained for long time periods by suitably orienting the sail plane in such a way that centrifugal and gravitational forces are balanced by the propelling thrust. For a given orbital period and a given sail performance (measured through its characteristic acceleration) it is possible to find the required values of orbital plane position, view angle and thrust angle. These results have been collected in graphical form to obtain a quick view of the electric sail capabilities. The problem of minimum time transfers towards a given non-Keplerian orbit has also been solved through an indirect approach. Finally, the problem of displaced orbit sensitivity to perturbations has been addressed by simulation.

For better emphasizing the electric sail performance, a comparison has been made with an ideal solar sail. From the obtained results, the electric sail appears as an intriguing alternative to a solar sail. Nevertheless, due to the substantial differences between the two propulsion systems, it is not possible to conclude whether an electric sail is superior or not to a solar sail, as long as missions involving displaced non-Keplerian orbits are concerned. In fact, a fair comparison requires a more accurate analysis of the electric sail subsystems. In particular, the availability of a parametric mass breakdown model is necessary to define a quantitative relationship between the electric sail characteristic acceleration and the deliverable payload mass.

References

Baoyin, H., Mcinnes, C. R.: Solar sail halo orbits at the Sun-Earth artificial L_1 point. Celest. Mech. Dyn. Astron. **94**(2), 155–171 (2006). doi:10.1007/s10569-005-4626-3

Brown, C.D.: Spacecraft mission design, pp. 71–73. AIAA Education Series (1992)

Bryson, A.E., Ho, Y.C.: Applied Optimal Control, Chap. 2, pp. 71–89. Hemisphere Publishing Corporation, New York, NY (1975)

Hughes, G.W., McInnes, C.R.: Solar sail hybrid trajectory optimization for non-Keplerian orbit transfers. J. Guid. Control Dyn. **25**(3), 602–604 (2002)

Janhunen, P., Sandroos, A.: Simulation study of solar wind push on a charged wire: basis of solar wind electric sail propulsion. Ann. Geophys. **25**(3), 755–767 (2007)

Kim, M., Hall, C.D.: Symmetries in the optimal control of solar sail spacecraft. Celest. Mech. Dyn. Astron. **92**(4), 273–293 (2005). doi:10.1007/s10569-004-2530-x

Kirpichnikov, S.N., Kirpichnikova, E.S., Polyakhova, E.N., Shmyrov, A.S.: Planar heliocentric roto-translatory motion of a spacecraft with a solar sail of complex shape. Celest. Mech. Dyn. Astron. **63**(3–4), 255–269 (2004). doi:10.1007/BF00692290

Koblik, V., Polyakhova, E., Sokolov, L.: Controlled solar sail transfers into near-sun regions combined with planetary gravity-assist flybys. Celest. Mech. Dyn. Astron. **86**(1), 59–80 (2003). doi:10.1023/A:1023626917595

McInnes, C.R.: The existence and stability of families of displacement two-body orbits. Celest. Mech. Dyn. Astron. **67**(2), 167–180 (1997). doi:10.1023/A:1008280609889

McInnes, C.R.: Passive control of displaced solar sail orbits. J. Guid. Control Dyn. **21**(6), 975–982 (1998)

McInnes, C.R.: Solar sailing: technology, dynamics and mission applications. Springer-Praxis series in space science and technology, pp. 175–196. Springer-Verlag, Berlin (1999)

McInnes, C.R., Brown, J.C.: The dynamics of solar sails with a non-point source of radiation pressure. Celest. Mech. Dyn. Astron. **49**(3), 249–264 (1990). doi:10.1007/BF00049416

McInnes, C.R., Simmons, J.F.L.: Solar sail halo orbits. Part I—heliocentric case. J. Spacecr. Rockets **29**(4), 466–471 (1992)

Mengali, G., Quarta, A.A.: Optimal control laws for axially symmetric solar sails. J. Spacecr. Rockets **42**(6), 1130–1133 (2005a)

Mengali, G., Quarta, A.A.: Time-optimal three-dimensional trajectories for solar photon thruster spacecraft. J. Spacecr. Rockets **42**(2), 379–381 (2005b)

Mengali, G., Quarta, A. A.: Compound solar sail with optical properties: models and performance. J. Spacecr. Rockets **43**(1), 239–245 (2006)

Mengali, G., Quarta, A.A.: Optimal heliostationary missions of high-performance sailcraft. Acta Astronaut. **60**(8–9), 676–683 (2007). doi:10.1016/j.actaastro.2006.07.018

Mengali, G., Quarta, A.A., Circi, C., Dachwald, B.: Refined solar sail force model with mission application. J. Guid. Control Dyn. **30**(2), 512–520 (2007). doi:10.2514/1.24779

Mengali, G., Quarta, A.A., Janhunen, P.: Considerations of electric sailcraft trajectory design. J. Br. Interplanet. Soc. **61**(8), 326–329 (2008a)

Mengali, G., Quarta, A.A., Janhunen, P.: Electric sail performance analysis. J. Spacecr. Rockets **45**(1), 122–129 (2008b). doi:10.2514/1.31769

Racca, G.D.: New challenges to trajectory design by the use of electric propulsion and other new means of wandering in the solar system. Celest. Mech. Dyn. Astron. **85**(1), 1–24 (2004). doi:10.1023/A:1021787311087

Stengel, R.F.: Stochastic Optimal Control: Theory and Applications, pp. 242–243. Wiley, New York, NY (1986)

Van Der Ha, J.C., Modi, V.J.: Long-term evaluation of three-dimensional heliocentric solar sail trajectories with arbitrary fixed sail setting. Celest. Mech. Dyn. Astron. **19**(2), 113–138 (1979). doi:10.1007/BF01796085

Wenzel, K.-P., Marsden, R.G., Page, D.E., Smith, E.J.: The Ulysses mission. Astron. Astrophys. Suppl. Ser. **92**(2), 207–219 (1992)

Wie, B.: Thrust vector control analysis and design for solar-sail spacecraft. J. Spacecr. Rockets **44**(3), 545–557 (2007). doi:10.2514/1.23084

Wright, J.L.: Space Sailing, pp. 223–226. Gordon and Breach Science Publisher, Berlin (1992)